The International Journal of Advanced Manufacturing Technology (2018) 99:1735–1753
https://doi.org/10.1007/s00170-018-2576-7

ORIGINAL ARTICLE

MQL milling of TC4 alloy by dispersing graphene into vegetable oil-based cutting fluid

Ming Li[1] · Tianbiao Yu[1] · Rongchuang Zhang[2] · Lin Yang[1] · Hongyu Li[1] · Wanshan Wang[1]

Received: 23 March 2018 / Accepted: 13 August 2018 / Published online: 25 August 2018

Abstract

Titanium alloy TC4 is widely used in aerospace, petrochemical, shipbuilding, automobile, and medicine due to its excellent comprehensive performances. However, TC4 is a difficult-to-machine material because of its low thermal conductivity, large friction coefficient, high chemical activity, and low elasticity modulus. In this paper, Minimum Quantity Lubrication (MQL) with vegetable oil-based cutting fluid was adopted in TC4 milling. Meanwhile, graphene nanoparticles were dispersed into the vegetable oil-based cutting fluid to improve the cooling and lubrication performances. In order to evaluate the performances, a series of milling experiments were conducted under the four cooling/lubrication conditions (dry, gas, pure MQL, and graphene MQL). The milling characteristics of TC4 in terms of milling force, milling temperature, tool wear, and surface integrity were compared. Results showed that the graphene additive was effective for improving the milling characteristics. Overall, the results could be explained that the graphene additive could enhance the cooling and lubrication performances of the oil film formed in the milling zone. The findings of this paper are expected to be meaningful to provide some experimental basis for the application of the graphene additive in MQL milling.

Keywords MQL milling · TC4 · Graphene · Vegetable oil-based cutting fluid · Milling characteristics

1 Introduction

As a hot research topic in machining, Minimum Quantity Lubrication (MQL) has been widely used in titanium alloy milling process [1]. Meanwhile, vegetable oil-based cutting fluids are widely adopted owing to good biodegradability, low environmental impact, and non-toxicity [2]. This technology could not only reduce the employed volume of cutting fluid but also enhance the ability to penetrate the cutting zone. Therefore, this is a very meaningful and promising technology.

To understand the cooling and lubrication characteristics of vegetable oil-based cutting fluids, many studies were conducted and reported. Changhe Li et al. [3] studied the lubrication properties of seven typical vegetable oils (castor oil, soybean oil, rapeseed oil, corn oil, sunflower oil, peanut oil, and palm oil) in MQL grinding of high-temperature nickel-based alloy. They stated that vegetable oil had better lubrication properties as compared to mineral oil and flood lubrication. This was because the oleic and ricinoleic acid contained in vegetable oil had high binding energy, low friction coefficient, and, therefore, better lubrication properties. Pervaiz et al. [4] researched the machining characteristics of titanium alloy under the vegetable oil-based MQL condition instead of the MWF-based conventional flood cooling method. Compared with dry cutting and conventional flood cooling, vegetable oil-based MQL condition provided better lubrication to reduce

✉ Tianbiao Yu
tianbiaoyudyx@gmail.com

Ming Li
limingeducn@163.com

Rongchuang Zhang
zhangrongchuang@mail.neuq.edu.cn

Lin Yang
jwdcmyl1011@gmail.com

Hongyu Li
m18640389373@163.com

Wanshan Wang
wws@mail.neu.edu.cn

[1] School of Mechanical Engineering and Automation, Northeastern University, Shenyang 110819, China

[2] School of Control Engineering, Northeastern University at Qinhuangdao, Qinhuangdao 066004, China

friction. Gajrani et al. [5] carried out a series of experiments to study the machining performances of bio-cutting fluid as compared to mineral oil. They stated that the MQL condition with bio-cutting fluid showed the better machining performances owing to the reduction of cutting zone contact length, higher viscosity, higher flash point, higher thermal conductivity, higher specific heat, and better ability to penetrate the chip-tool interface. Khan et al. [6] investigated the influences of vegetable oil-based cutting fluid on cutting performances in MQL turning of low alloy steel AISI 9310. They concluded that MQL with vegetable oil-based cutting fluid reduced average chip-tool interface temperature up to 10% and improved chip formation modes, tool wear, and surface finish in varying degrees as compared to flood machining. Priarone et al. [7] studied the effects of lubrication strategy on machining performances in the milling of titanium aluminide. Lower flank wear, higher tool life, and lower average surface roughness (0.1 μm, 80 min, 0.5 μm respectively) were achieved under the vegetable oil MQL condition. Rahim et al. [8] conducted a series of experiments to study the machining performances of palm oil and synthetic ester under MQL drilling of Ti-6Al-4 V with uniform cutting parameters as compared to air blow and flood conditions. They stated that palm oil had the best performance thanks to the formation of thin boundary lubrication film which reduced the friction and heat in tool-workpiece and tool-chip interface.

In addition, in order to further improve the cooling and lubrication performances, various nanoparticles were dispersed into traditional cutting fluids based on the theory of solid enhancing heat transfer [9]. Meanwhile, the investigations on the cooling and lubrication mechanisms were conducted to improve the machining characteristics.

To understand the cooling and lubrication characteristics of nanoparticle-dispersed cutting fluids, many studies were conducted and reported. These studied nanoparticle additives mainly include four types, such as metals, metal oxides, metal sulfide, and carbide [10, 11]. Padgurskas et al. [12] dispersed Fe, Cu, and Co nanoparticles into mineral oil and investigated tribological properties by a series of tribological tests. They concluded that nanoparticles significantly decreased the friction coefficient and wear of friction pairs and Cu nanoparticles achieved the most effective reduction of friction and wear. Shabgard et al. [13] added CuO to vegetable oil (canola oil) to synthesize the nanofluid and cooling and lubrication properties of copper oxide nanofluids were evaluated in surface grinding of AISI 1045 hardened steel. They stated that the synthesized nanofluids significantly decreased the grinding forces and temperatures and improved surface integrity. Lee et al. [14] prepared the nanofluids by added nanodiamond and Al_2O_3 nanoparticles to paraffin oil respectively to evaluate the micro-grinding characteristics of tool steel. They stated that nanodiamond-dispersed cutting fluid was more effective as compared to Al_2O_3 nanoparticle-dispersed cutting fluid for decreasing grinding force and Al_2O_3 nanoparticle-dispersed cutting fluid was more effective as compared to nanodiamond-dispersed cutting fluid for decreasing surface roughness. Kalita et al. [15] impregnated MoS2 nanoparticles to mineral oil (paraffin) and vegetable oil (soybean oil) to prepare nanofluids respectively and evaluated their tribological properties in surface grinding of cast iron and EN24 alloy steel. They confirmed that the nanofluids improved the process efficiency owing to the reduction of friction and energy dissipation in MQL grinding and had a better performance as the concentration of nanoparticles increases. Changhe Li et al. [16] added carbon nanotube (CNT) nanoparticles to palm oil to prepare nanofluids and evaluated their cooling and lubrication performances in MQL grinding of the Ni-based alloy. They stated that the higher thermal conductivity of nanofluids was helpful in enhancing heat transfer; higher viscosity of nanofluids was conducive to improving the lubrication effect and reducing energy input and heat generation. Kim et al. [17] added nanodiamond particles to vegetable oil to prepare the nanofluid under the micro-end-milling process of titanium alloy (Ti6Al4V). They concluded that the lower concentration of nanodiamond nanofluid (0.1 wt.%) was more conducive to decreasing the milling force, friction coefficient and tool wear and the higher concentration (1.0 wt.%) was more effective to reduce the surface roughness. Park et al. [18] dispersed exfoliated graphite nanoplatelets (xGnps) into vegetable oil to form nanofluids during MQL ball milling. They concluded that xGnps-dispersed vegetable oil showed remarkable performances, especially in central wear and chipping at the cutting edge. Yu Su et al. [19] impregnated graphite to the vegetable-based oil (LB2000) and unsaturated polyol ester (PriEco6000) to prepare nanofluids respectively and investigated the machining performances in the cylindrical turning of AISI 1045 medium carbon steel. They concluded that the nanofluids decreased cutting force and temperature significantly and graphite-LB2000 nanofluid outperformed graphite-PriEco6000 nanofluid, especially at a high cutting speed. In addition, some other nanoparticles were also added to the cutting fluids, such as ZrO_2 [20], carbon onions [21], polycrystal diamond [20], and SiO_2 [22, 23].

However, although many researchers have dispersed a variety of nanoparticles into cutting fluids and studied their cooling and lubrication properties, only a few dispersed graphene nanoparticles into vegetable oil-based cutting fluids. Graphene has excellent thermal conductivity (thermal conductivity up to 5300 W/(m K)) and very good lubrication properties, which the first two-dimensional material discovered and the highest thermal conductivity carbon material so far [24, 25]. In addition, TC4 is a difficult-to-machine material thanks to its low thermal conductivity, large friction coefficient, high chemical activity, low elasticity modulus, high strength at elevated temperature, and high mechanical resistance, and the vegetable oil-based cutting fluid with better cooling and

lubrication performances is required in TC4 MQL milling [26]. Therefore, graphene is a promising additive for cutting fluids to improve cooling and lubrication performances in TC4 MQL milling.

To fill this gap, in this study, graphene-dispersed vegetable oil-based cutting fluid was prepared and its cooling and lubrication properties were evaluated. By conducting systematic experiments, special emphasis is laid on the effects of the graphene additive in terms of milling force (time domain analysis, frequency domain analysis), milling temperature (surface temperature, subsurface temperature), tool wear (tool life, tool flank wear, and the maximum width of the tool flank wear-land), and surface integrity (surface morphology, surface roughness, surface micro-hardness, and subsurface micro-hardness) in the four cooling/lubrication conditions (dry, gas, pure MQL, graphene MQL). The cooling and lubrication mechanisms were discussed by experimental results. The findings of this study are expected to promote the application of the graphene additive in cutting fluids and provide certain technical references for industrial application.

2 Experiment

In this study, the milling experiments in the four cooling/lubrication conditions (dry, gas, pure MQL, graphene MQL) were conducted respectively. The milling characteristics of TC4 in terms of milling force, milling temperature, tool wear, and surface integrity were evaluated respectively.

2.1 Two-step preparation of graphene-dispersed cutting fluid

The preparation methods of nanoparticle-dispersed cutting fluid mainly include the one-step method and two-step method [27, 28]. In the one-step method, the preparations of the nanoparticles and nanoparticle-dispersed cutting fluids are performed synchronously, i.e., the nanoparticles are uniformly dispersed into the cutting fluid at the same time that the nanoparticles are prepared. However, the process is very complicated, expensive, and, therefore, not suitable for industrial applications. In the two-step method, the prepared nanoparticles are dispersed into a cutting fluid to prepare the nanoparticle-dispersed cutting fluid, i.e., the preparations of nanoparticles and nanoparticle-dispersed cutting fluids are not performed at the same time. In addition, the process is simple, relatively inexpensive, and, therefore, suitable for industrial applications. Therefore, in this study, the graphene-dispersed cutting fluids were prepared by using the two-step method.

In this paper, the few-layer graphene was used as the additive, as shown in Fig. 1. The average layer thickness of the graphene is less than 5 nm with a mean diameter of 10 μm. The vegetable oil-based cutting fluid LB2000 (supplied by ITW Rocol North America Co., Ltd.) was chosen as base fluid owing to good biodegradability, low environmental impact, and non-toxicity. The properties of graphene and LB2000 are given in Tables 1 and 2, respectively. The high-precision electronic scale was used to weigh the graphene nanoparticle and vegetable oil-based cutting fluid. This type of electronic scale has a range of 200 g and an accuracy of 0.001 g, as shown in Fig. 2.

The graphene-dispersed cutting fluid was prepared by dispersing a certain amount of graphene into LB2000 with the weight concentration of 0.1 wt.% by the two-step method. As shown in Fig. 2, the cutting fluid was first stirred on a magnetic stirrer (for 30 min) and then ultra-sonicated by an ultrasonic dispersion instrument (40 kHz, 80 W) (for 1 h). The process was repeated several times until all the graphene nanoparticles were dispersed consistently in LB2000. The graphene-dispersed cutting fluid was steady and an obvious sedimentation phenomenon was not observed after standing for 12 h, as shown in Fig. 3. In addition, the sedimentation phenomenon was also not observed during the entire experiment process.

2.2 Workpiece material and cutting tool

In this study, the titanium alloy TC4 was adopted in the following experiments. The workpiece was cut into the rectangular solid with the dimension 80 mm (length) × 30 mm (width) × 15 mm (height) by WEDM machine. Prior to the experiments, the surface oxidation layer of the workpiece was removed by grinding and the heat-affected layer was removed by using a solution containing 5% hydrofluoric acid and 20% nitric acid. The chemical composition and mechanical properties of the workpiece are depicted in Tables 3 and 4, respectively.

TC4 is a difficult-to-machine material thanks to its low thermal conductivity, large friction coefficient, high chemical activity, low elasticity modulus, high strength at elevated temperature, and high mechanical resistance. The carbide tool is suitable for cutting TC4 alloy because the carbide tool has high hot hardness, good toughness, good wear resistance, high thermal conductivity, low chemical activity, and good impact resistance [29]. The cutting tools adopted in the following experiments were solid carbide end mill (GM-4E-D6.0, Zhuzhou cemented carbide Group Co., Ltd.) with a diameter of 6 mm, a length of 50 mm, a spiral angle of 45° and four flutes. The matrix material and the coating material of the cutting tools were ultra-fine tungsten steel and TiAlN, respectively. The detailed information of the milling tool is shown in Table 5.

2.3 Machine tool and MQL system

In this study, all the experiments were conducted on a four-axis vertical milling machining center (TH5650, Shenyang machine tool (Group) Co., Ltd.), as illustrated in Fig. 4b. The numerical control system of TH5650 was FANUC 0i-MB. The main technical parameters were as follows: the total power of 35 KW, the maximum spindle

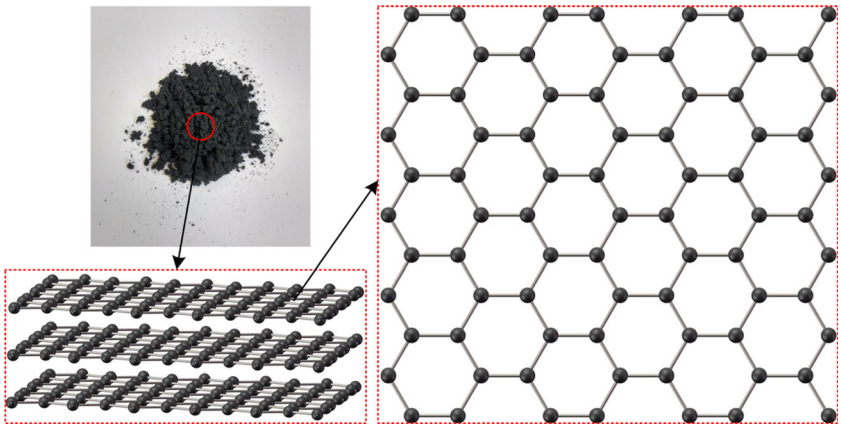

Fig. 1 The structure diagram of few-layer graphene

speed of 6000 rpm, and the working range ($X \times Y \times Z$) of 850 mm × 500 mm × 630 mm.

In addition, MQL milling experiments were conducted using Accu-Lube MQL system (supplied by ITW Rocol North America Co., Ltd.). This system was mainly composed of an air pump, filter, pulse generator, pulse pump, oil tank, and oil-gas mixing tube, as illustrated in Fig. 4c. The compressed air at a certain pressure is mixed with a certain amount of cutting fluid discharged by the pulse pump and then injected into the cutting zone. The pressure of the compressed air and the flow rate of the cutting fluid are regulated by the air pump and pulse pump respectively. The flow rate of the cutting fluid (Q) is measured by measuring the change in volume of the cutting fluid in the tank over a period of time, as shown in Fig. 5 and Eq. (1). In this study, the parameters of the MQL system under the pure MQL and graphene MQL condition were the same. The main technical parameters were as follows: the MQL flow rate of 60 mL/h and the MQL gas pressure of 6.0 bar.

$$\begin{aligned} Q &= \frac{V_1 - V_2}{t_2 - t_1} \\ &= \frac{\left[\pi\left(\frac{D}{2}\right)^2 h_1 - \pi\left(\frac{d}{2}\right)^2 h_1\right] - \left[\pi\left(\frac{D}{2}\right)^2 h_2 - \pi\left(\frac{d}{2}\right)^2 h_2\right]}{t_2 - t_1} \\ &= \frac{\pi\left(D^2 - d^2\right)(h_1 - h_2)}{4(t_2 - t_1)} \end{aligned} \tag{1}$$

2.4 Experimental scheme

Milling force, milling temperature, tool wear, and surface integrity are vital evaluation parameters in the milling process. In this section, a series of experiments was designed to evaluate milling force, milling temperature, tool wear, and surface integrity under the dry, gas, pure MQL, and graphene MQL condition. Meanwhile, in order to reduce the error, each experiment was repeated 30 times. In this study, the gas condition is that only high-pressure gas is injected into the cutting zone, namely the cutting fluid flow rate of the MQL system is zero under the gas condition. In the MQL milling, the high-pressure gas and cutting fluid are mixed and injected into the cutting zone. Meanwhile, the high-pressure gas and cutting fluid have a certain impact on the milling performances. Therefore, it is necessary to introduce the gas condition to evaluate the effects of the high-pressure gas on the milling performances. In the milling process, the slot milling (i.e., full immersion milling) is a symmetrical milling method that could reduce the effects of tool runout on the milling process [30]. In this study, in order to reduce the effects of tool runout on milling force and tool wear, the slot milling strategy (i.e., the full immersion milling) was chosen to evaluate milling force and tool wear. Meanwhile, in order to measure the milling temperature and surface integrity more conveniently, the side milling strategy (i.e., the partial immersion milling) was chosen to evaluate milling temperature and surface integrity, as shown in Fig. 6.

2.4.1 Evaluation of milling force

A series of slot milling experiments were designed to evaluate the effects of the cooling/lubrication condition on milling force. The main milling parameters included the spindle rotation speed ($N = 796$ rpm), the feed rate per tooth ($f_z =$ 0.016 mm/z), and the axial immersion depth ($a_p = 0.1$ mm). As seen in Fig. 4a, the measurement of milling force was carried out along the x-axis, y-axis, and z-axis by using a 3D force-measuring system (9257B, Kistler Co., Ltd), which

Table 1 The properties of graphene

Property	Average layer thickness (nm)	Mean diameter (μm)	Number of layers	Specific surface area (m^2/g)	Appearance
Value	< 5	10	1–5	360–450	Black powder

Table 2 The properties of LB2000

Property	Density (at 20 °C) (g/cm^3)	Flash point (°C)	Pour point (°C)	Appearance
Value	0.92	320	− 20	Dark blue fluid

includes a three-component dynamometer, a multichannel charge amplifier, an A/D data acquisition card, and a PC. The sampling frequency of milling force was set at 4000 Hz. Evaluations of milling force were carried out in the time domain and frequency domain, respectively.

For the time domain analysis, the milling force curves under the four cooling/lubrication conditions were compared. Moreover, a statistical analysis was made on the positive and negative peak of measured milling force curves according to Eq. (2) to quantify the effects of the cooling/lubrication condition on the milling force.

$$\begin{aligned}\overline{F_{xm}} &= \frac{F_{xm}^{+} + F_{xm}^{-}}{2} \\ \overline{F_{ym}} &= \frac{F_{ym}^{+} + F_{ym}^{-}}{2} \\ \overline{F_{zm}} &= \frac{F_{zm}^{+} + F_{zm}^{-}}{2}\end{aligned} \tag{2}$$

For the frequency domain analysis, the frequency spectra of the milling force signals were transformed by the Fast Fourier Transforms (FFT) method. The dominant frequency structure of the frequency spectrum is usually characterized by the spindle rotation frequency (SRF), the tooth passing frequency (TPF) and their corresponding higher order harmonics in the stable milling process [31, 32]. SRF and TPF are defined using the following equations:

$$SRF = \frac{N}{60} \tag{3}$$

$$TPF = zgSRF = \frac{zN}{60} \tag{4}$$

where N is the spindle rotation speed (in rpm) of the machine tool, and z is the tooth number of the milling tool. The amplitude of the dominant frequency in the frequency spectrum could represent the vibration intensity of the milling process. Therefore, we could evaluate the vibration state in the milling process by the amplitude of the dominant frequency [33].

2.4.2 Evaluation of milling temperature

Milling temperature directly affects the workpiece surface integrity and tool wear. In this study, the surface temperature and the subsurface temperature of the workpiece were measured. A series of milling experiments was designed to evaluate the effects of the cooling/lubrication condition on milling temperature. The main milling parameters included the spindle rotation speed (N = 796 rpm), the feed rate per tooth (f_z = 0.04 mm/z), the radial immersion depth (a_e = 0.2 mm), and the axial immersion depth (a_p = 0.2 mm).

The measurement strategy diagram of the surface temperature is shown in Fig. 7a. A commercial K-type thermocouple (TT-K-36-SLE, OMEGA) was inserted into a 0.30-mm-diameter hole in the workpiece to measure the surface temperature. Meanwhile, the measurement strategy diagram of the subsurface temperature is shown in Fig. 7b. A commercial K-type armored thermocouple probe (WRNK-191, YUSHENG) was inserted into a 1.0-mm-diameter hole in the workpiece to measure the subsurface temperature. As shown in Fig. 7, the K-type thermocouple and K-type armored thermocouple probe were all held by using two identical workpieces. Meanwhile, the two workpieces are positioned by the positioning pins to reduce the errors for inconsistent placement. In addition, the 0.3-mm-diameter thermocouple mounting hole is composed of two 0.3-mm-diameter circular slots, and the 1.0-mm-diameter thermocouple mounting hole is composed of two 1.0-mm-diameter circular slots. As shown in Fig. 8, the 0.3-mm-diameter circular slot is prepared by the micro ball end mill (R0.15 mm), and the 1.0-mm-diameter circular slot is prepared by the micro ball end mill (R0.5 mm). In addition, the temperature signals were processed by a multichannel signal

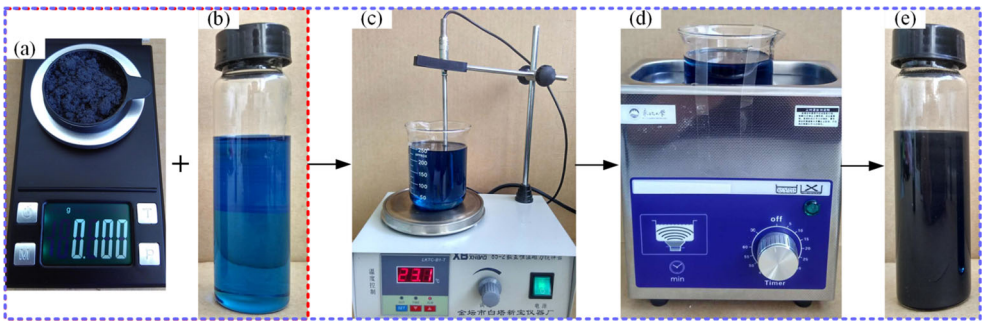

Fig. 2 The preparation process of graphene-dispersed cutting fluid ((**a**) the few-layer graphene and high precision electronic scale, (**b**) pure LB200, (**c**) magnetic stirrer, (**d**) ultrasonic dispersion instrument, and (**e**) graphene-dispersed cutting fluid)

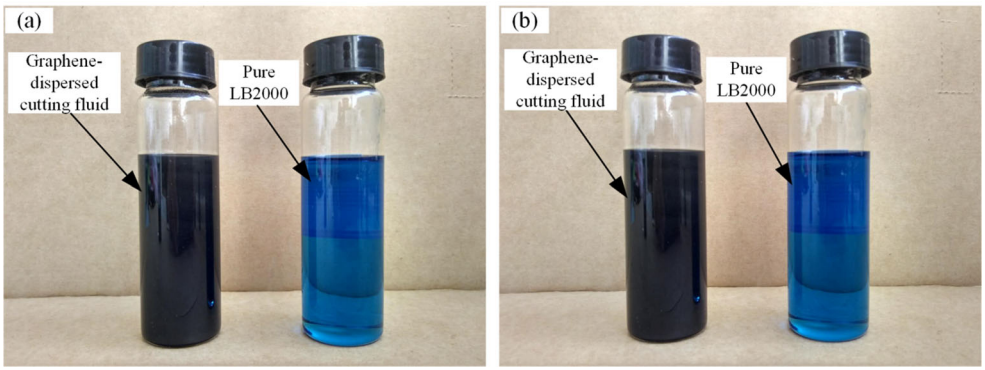

Fig. 3 The static observation of the graphene-dispersed cutting fluid ((**a**) prepared freshly and (**b**) after standing for 12 h)

processing system and displayed on the temperature measurement software installed on the computer. The sampling frequency of milling temperature was set at 20 KHz.

2.4.3 Evaluation of tool wear

Tool wear directly affects the machining quality, machining efficiency, and machining costs. In this section, in order to evaluate the effects of the cooling/lubrication condition on tool wear, the tool life under the four cooling/lubrication conditions (dry, gas, pure MQL and graphene MQL) were studied by conducting a series of slot milling experiments. The main milling parameters included the spindle rotation speed (N = 796 rpm), the feed rate per tooth (f_z = 0.016 mm/z) and the axial immersion depth (a_p = 0.1 mm). The tool flank wear was observed by the laser confocal microscope (LEXT OLS4100, Japan Olympus Corporation) at every 880 mm of milling length, as shown in Fig. 9a. Meanwhile, the maximum width of the tool flank wear-land (VB_{max}) was measured. In addition, the tool wear under the four cooling/lubrication conditions were compared and analyzed when the milling length is 5280 mm because the tool wear under the four cooling/lubrication conditions were all in a relatively stable state at this time.

2.4.4 Evaluation of surface integrity

Surface integrity directly determines the use performance and reliability of the workpiece. A series of milling experiments was designed to evaluate the effects of the cooling/lubrication condition on surface integrity. The main milling parameters included the spindle rotation speed (N = 796 rpm), the feed rate per tooth (f_z = 0.04 mm/z), the radial immersion depth (a_e = 0.2 mm), and the axial immersion depth (a_p = 0.2 mm).

The machined surfaces under the four cooling/lubrication conditions were observed by the laser confocal microscope (LEXT OLS4100, Japan Olympus Corporation), as shown in Fig. 9a. Meanwhile, the surface roughness of the machined surface was measured. In addition, the surface micro-hardness and subsurface micro-hardness with the depth increasing to 200 μm under the four cooling/lubrication conditions were measured on the polished machined surface and cross section by the micro-hardness tester (TUKON1102, Wilson) with an indenter load of 20 gf and a holding time of 10 s, respectively. The subsurface micro-hardness was measured on the cross section, the distance between the first indentation used to measure the subsurface micro-hardness and the machined surface was 20 μm, and each indentation width was 20 μm, as shown in Fig. 10. Meanwhile, the depth of the subsurface hardening layer was measured by the laser confocal microscope.

3 Experimental results and discussions

In this section, the experimental results under the four cooling/lubrication conditions (dry, gas, pure MQL, graphene MQL) were provided. The milling characteristics of TC4 and the effects of the graphene additive in terms of milling force, milling temperature, tool wear, and surface integrity were discussed.

3.1 Milling force

Milling force is a vital evaluation parameter in the milling process. It indicates the interaction between milling tool and work material and directly affects surface quality, machining accuracy, milling temperature, and tool life. Therefore, it is necessary to study the milling force of TC4 under different cooling and lubrication conditions.

Table 3 The chemical composition of TC4

Element	Ti	Fe	C	N	H	O	Al	V
Composition (wt.%)	Balance	0.30	0.10	0.05	0.015	0.20	5.5–6.8	3.5–4.5

Table 4 The mechanical properties of TC4

Property	Tensile strength (MPa)	Yield strength (MPa)	Elongation (%)	Poison ratio	Modulus of elasticity (GPa)	Hardness (HV)
Value	990	830	14	0.342	114	312

In order to estimate the effects of the graphene additive on milling force, a series of slot milling experiments was carried out. The measured typical signal diagrams of milling force under the four cooling/lubrication conditions are shown in Fig. 11. In order to quantify the effects of the cooling/lubrication condition on the milling force, a statistical analysis was made on the positive and negative peak of measured milling force, as shown in Fig. 12. The milling force of the four cooling/lubrication conditions was compared. The $\overline{F_{xm}}$, $\overline{F_{ym}}$, and $\overline{F_{zm}}$ under the dry condition are 13.47 N, 15.41 N, and 8.15 N, respectively. The gas condition has the milling force of $\overline{F_{xm}}$ = 13.03 N, $\overline{F_{ym}}$ = 14.04 N, and $\overline{F_{zm}}$ = 7.65 N, which is 3.27%, 8.89%, and 6.13% smaller than those of the dry condition, respectively. The pure MQL condition yields the milling force of $\overline{F_{xm}}$ = 10.81 N, $\overline{F_{ym}}$ = 11.87 N, and $\overline{F_{zm}}$ = 7.32 N, which is 19.75%, 22.97%, and 10.18% smaller than those of the dry condition, respectively. The graphene MQL condition shows the milling force of $\overline{F_{xm}}$ = 8.84 N, $\overline{F_{ym}}$ = 9.65 N, and $\overline{F_{zm}}$ = 6.68 N, which is 34.37%, 37.38%, and 18.04% smaller than those of the dry condition, respectively.

Compared with the dry condition, the milling forces under the pure MQL and graphene MQL condition are significantly reduced. It is believed that the lubricating oil film formed in the milling zone shows a good anti-friction and load-bearing capacity (see Fig. 19). The milling force under the graphene MQL condition is smaller than that under the pure MQL condition. This is likely because the graphene additive could enhance the anti-friction and load-bearing capacity of the oil film formed in milling zone (see Fig. 19c). Compared with the pure MQL and graphene MQL condition, the effect of the gas condition on the milling force is slightest. This may be due to insufficient lubrication in the milling zone under the gas condition (see Fig. 19a).

In addition, the frequency domain analysis of the measured milling force signals was carried out to further explore the effects of the cooling/lubrication condition on milling force and vibration in the milling process. As the spindle rotation speed (N) of the machine tool is 796 rpm and the tooth number (z) of milling tool is 4, the spindle rotation frequency (SRF) and the tooth passing frequency (TPF) are 13.27 Hz and 53.07 Hz, respectively. As shown in Fig. 13, the dominant frequency structure of the frequency spectra is characterized by the spindle rotation frequency (SRF), the tooth passing frequency (TPF) and their corresponding higher order harmonics. This indicates that the vibration information contained in the milling force signals is mainly caused by tooth passing and spindle rotation. In contrast with the dry condition, the amplitudes of the SRF and the TPF under the pure MQL and graphene MQL condition are significantly reduced. This can be considered that the vibration intensity of the milling process under the pure MQL and graphene MQL condition is significantly reduced. This shows that the lubricating oil film formed in the milling zone not only reduces the vibration intensity caused by the tooth passing but also reduces the vibration intensity caused by the spindle rotation. This can be explained that the lubricating oil film formed in the milling zone shows a damping effect except for the anti-friction and load-bearing capacity. The amplitudes of the SRF and the TPF under the graphene MQL condition are smaller than those under the pure MQL condition. This is likely due to the fact that the graphene additive could enhance the damping effect of the oil film formed in milling zone. Compared with the pure MQL and graphene MQL condition, the effect of the gas condition on the amplitudes of the SRF and the TPF is slightest. This may be due to the fact that the oil film is not formed in the milling zone under the gas condition.

Table 5 The detailed information of the milling tool

Property	Value
Diameter (mm)	6
Total length (mm)	50
Cutting edge length (mm)	16
Number of flutes	4
Coating	TiAlN
Matrix material	Ultra-fine tungsten steel
Helix angle (°)	45
Rake (°)	8
Relief angle (°)	14

3.2 Milling temperature

Milling temperature is also a vital evaluation parameter in the milling process. This is because the milling temperature directly affects the workpiece surface integrity and tool life. Hence, it is necessary to study the milling temperature of TC4 under different cooling/lubrication conditions.

The measured typical signal profiles of the surface temperature and the subsurface temperature in the milling experiments under the four cooling/lubrication conditions are depicted in Fig. 14. It should be noted that these temperature

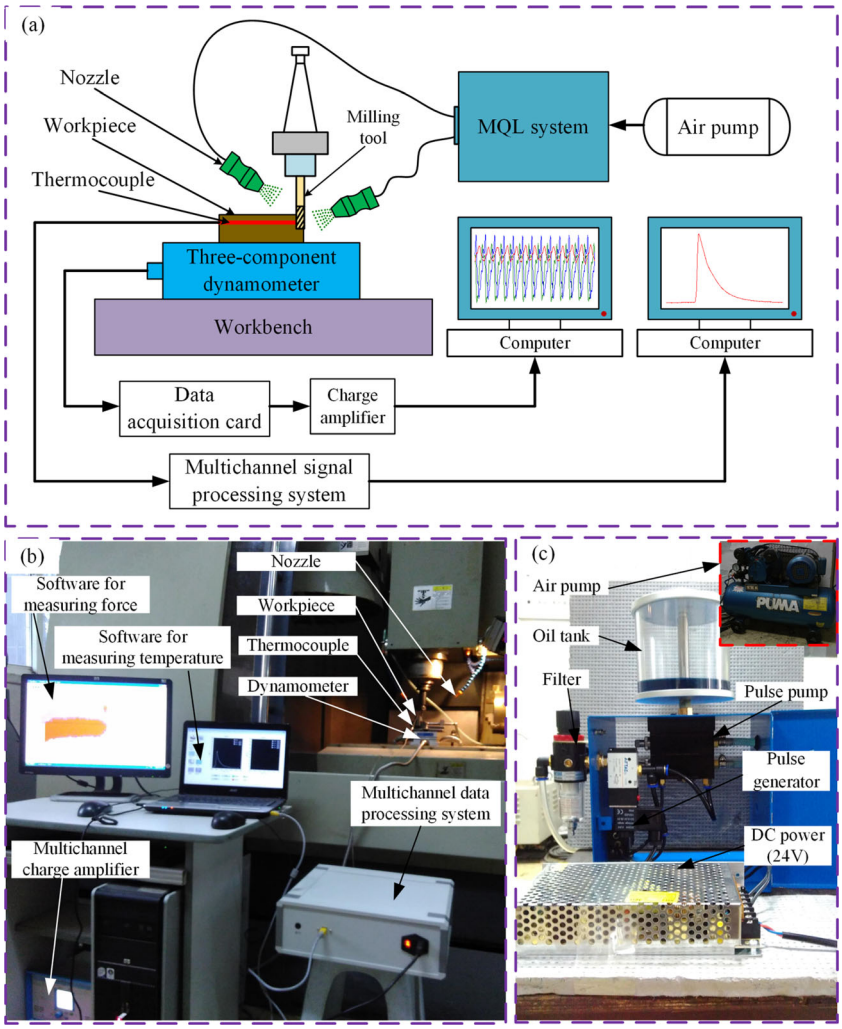

Fig. 4 Milling experiment diagram ((**a**) experiment schematic, (**b**) measurement system and (**c**) MQL system)

signals have been filtered. The graphene MQL condition yields the highest milling temperature, while the dry condition has the lowest milling temperature. It is obvious that the temperature measured on the surface is higher than that measured on the subsurface under each cooling/lubrication condition. Obviously, all of the measured temperature profiles include four stages, whether the surface temperature profiles or the subsurface temperature profiles. In the milling experiments, the temperature reaches the peak stage from room temperature through a rapid rise stage, and then reaches the room temperature after a rapid reduction stage and a slow reduction stage. In order to quantify the effects of cooling/lubrication conditions on the milling temperature, the measured milling temperature peaks were compared. The temperature peaks and the difference between the surface temperature peak and the subsurface temperature peak under the four cooling/lubrication conditions are shown in Fig. 15. The surface temperature peak and the subsurface temperature peak under the dry condition

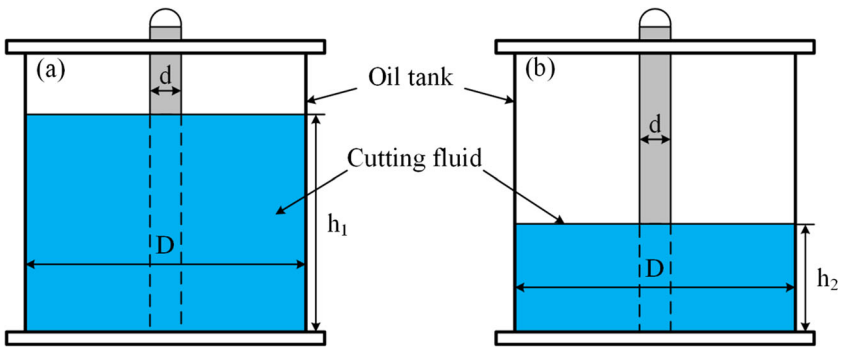

Fig. 5 The measurement principle of the flow rate ((**a**) at time t_1, (**b**) at time t_2)

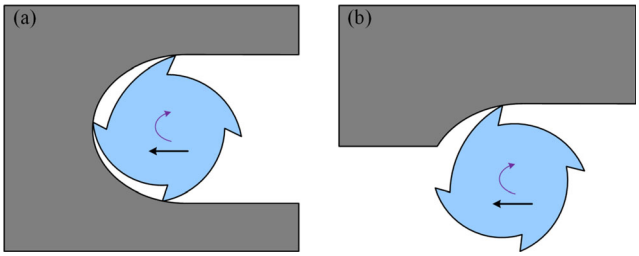

Fig. 6 The milling strategy ((**a**) the slot milling strategy, (**b**) the side milling strategy)

are 247.01 and 224.13 °C, respectively. The surface temperature peak and the subsurface temperature peak under the gas condition are 241.48 and 220.01 °C, which is 2.23% and 1.84% smaller than those of the dry condition, respectively. The surface temperature peak and the subsurface temperature peak under the pure MQL condition are 204.59 and 189.41 °C, which is 17.17% and 15.49% smaller than those of the dry condition, respectively. The surface temperature peak and the subsurface temperature peak under the graphene MQL condition are 173.14 and 165.75 °C, which is 29.91% and 26.05% smaller than those of the dry condition, respectively. In addition, the difference between the surface temperature peak and the subsurface temperature peak under the dry condition is 22.87 °C. Among the four cooling/lubrication conditions, the dry condition shows the largest difference. The difference between the surface temperature peak and the subsurface temperature peak under the gas condition, pure MQL, and graphene MQL condition are 21.47, 15.18, and 7.40 °C, which is 6.12%, 33.62%, and 67.64% smaller than that of the dry condition, respectively.

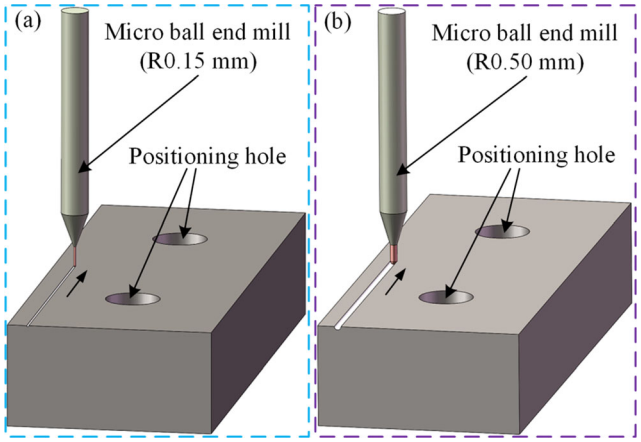

Fig. 8 The preparation strategy of thermocouple installation hole ((**a**) the 0.30-mm-diameter hole and (**b**) the 1.0-mm-diameter hole)

In contrast to the dry condition, both milling temperature and the difference between the surface temperature peak and the subsurface temperature peak under the pure MQL and graphene MQL condition are significantly reduced. It is believed that the lubricating oil film formed in the milling zone shows a good cooling capacity. The milling temperature under the graphene MQL condition is smaller than that under the pure MQL condition. Meanwhile, the difference between the surface temperature peak and the subsurface temperature peak under the graphene MQL condition is also smaller than that under the pure MQL condition. This is likely because the graphene additive could enhance the cooling capacity of the oil film formed in milling zone based on the theory of solid enhancing heat transfer. The effect of the gas condition on the

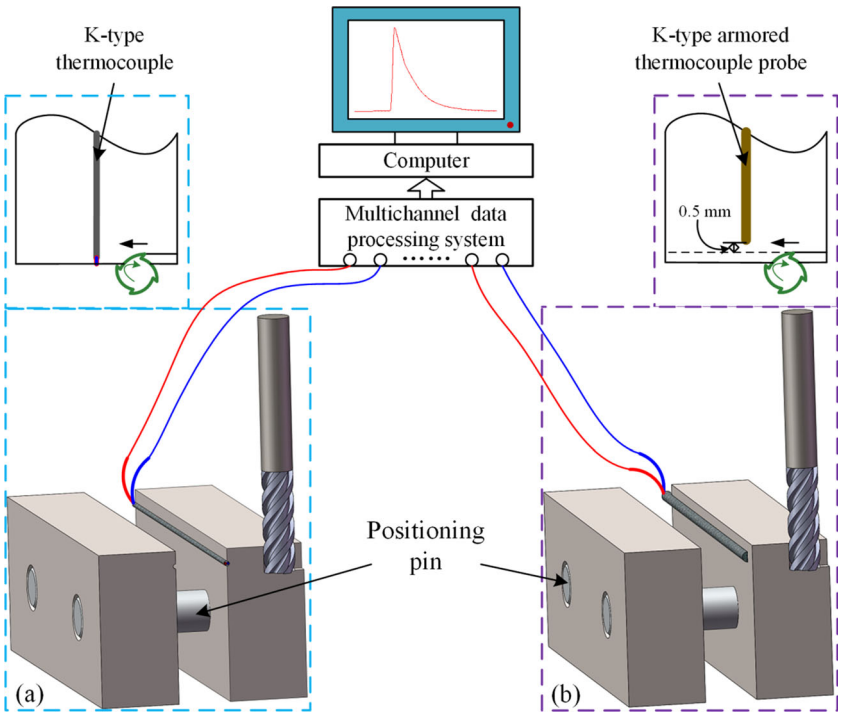

Fig. 7 The measurement strategy diagram of milling temperature ((**a**) the surface temperature measurement and (**b**) the subsurface temperature measurement)

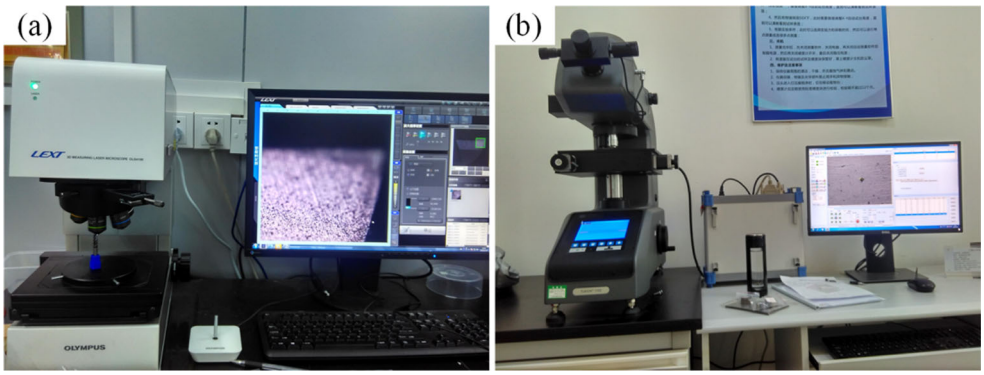

Fig. 9 The testing equipment for surface integrity ((**a**) laser confocal microscope and (**b**) micro-hardness tester)

milling temperature is slightest compared with the pure MQL and graphene MQL condition. This may be due to insufficient cooling in the milling zone under the gas condition.

3.3 Tool wear

The tool wear directly affects the milling force, the milling temperature, and the surface integrity of the workpiece in the milling process. Hence, the tool wear is also a very important evaluation parameter. Reducing tool wear can effectively improve the machining efficiency, reduce the machining cost, and improve the machining quality. Therefore, it is necessary to study the effects of different cooling/lubrication conditions on tool wear.

The tool life curves under the four cooling/lubrication conditions are shown in Fig. 16. The tool wear trends under the four cooling/lubrication conditions are similar, i.e., the tool wear goes through a period of sharp increase before it enters a relatively steady state and then enters a sharp deterioration stage until the tool fails. The tool life in the dry condition is 7920 mm, which is the smallest under the four cooling/lubrication conditions. Under the gas, pure MQL, and graphene MQL condition, the tool life is 8800; 11,440; and 14,080 mm, which is 11.11%, 44.44%, and 77.78% larger than that of the dry condition, respectively. When the milling length reached 5280 mm, the tool flank wear under the four cooling/lubrication conditions was observed and analyzed. Confocal microscope photos of the milling tool flank for the four cooling/lubrication conditions are given in Fig. 17. In the dry and gas condition, adhesion, edge chipping and built-up edge were observed. However, only less adhesion was observed under the pure MQL and graphene MQL condition. Obviously, edge chipping, built-up edge, and larger adhesion were almost nonexistent in the pure MQL and graphene MQL condition. The tool flank wear under the dry and gas condition was much more serious than that in the pure MQL and graphene MQL condition. In order to quantify the effects of the cooling/lubrication condition on the tool wear, the maximum width of the tool flank wear-land (VB_{max}) was measured. The maximum width of the tool flank wear-land under the four cooling/lubrication conditions were compared, as shown in Fig. 18. The maximum width of the tool flank wear-land in the dry condition is 187 μm, which is the largest under the four cooling/lubrication conditions. Under the gas, pure MQL and graphene MQL condition, the maximum width of the tool flank wear-land is 175, 140, and 129 μm, which is 6.42%, 25.13%, and 31.02% smaller than that of the dry condition, respectively.

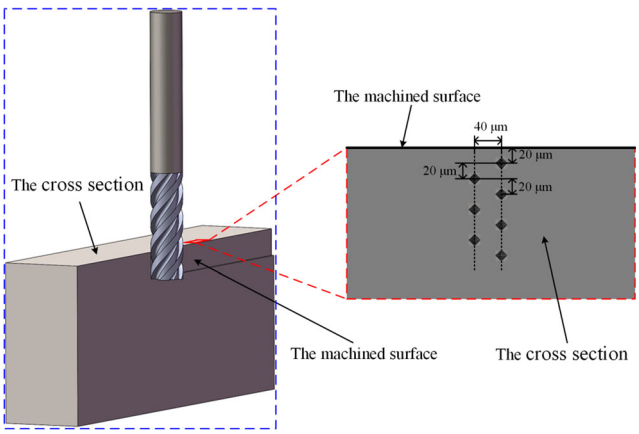

Fig. 10 The micro-hardness testing strategy

Among the four cooling/lubrication conditions, the dry condition achieves the largest tool wear; by contrast, the graphene MQL condition shows the smallest tool wear. Meanwhile, under the dry and gas condition, the phenomenon of adhesion, edge chipping, and built-up edge was obvious, while there was only less adhesion in the pure MQL and graphene MQL condition. This result is in agreement with those of milling force and milling temperature, which are described in Section 3.1 and Section 3.2. This is because the larger milling force and milling temperature are more likely to cause the larger tool wear, namely the larger milling force could cause the edge chipping, and the larger milling temperature could cause adhesion and built-up edge. Under the pure MQL and graphene MQL condition, the oil film, which providing sufficient lubrication and cooling in the milling zone, could lead to the reduction of edge chipping and built-up edge. Meanwhile, the oil film formed in the milling zone could also

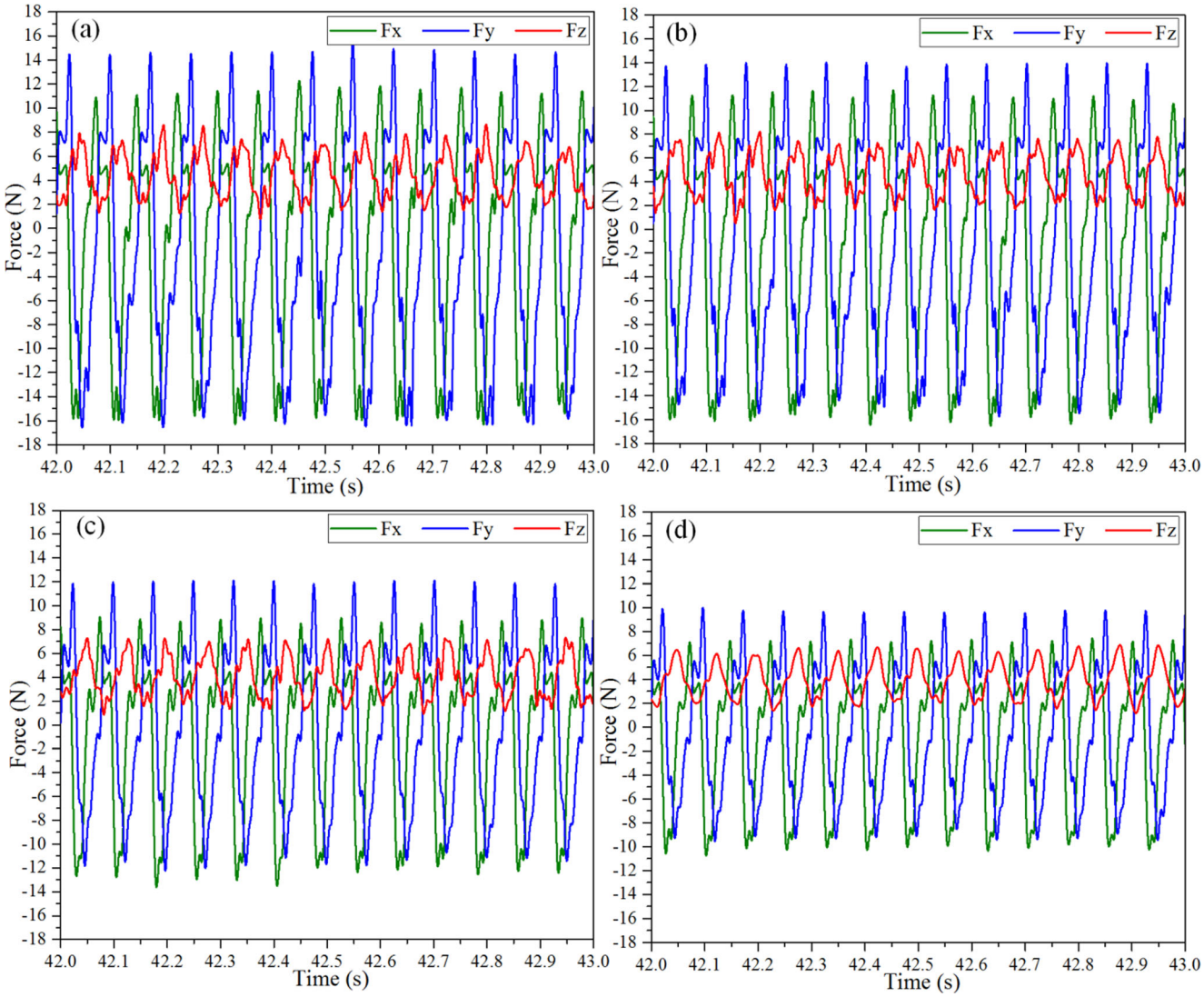

Fig. 11 The measured typical signal diagrams of milling force under the four cooling/lubrication conditions ((**a**) dry, (**b**) gas, (**c**) pure MQL and (**d**) graphene MQL)

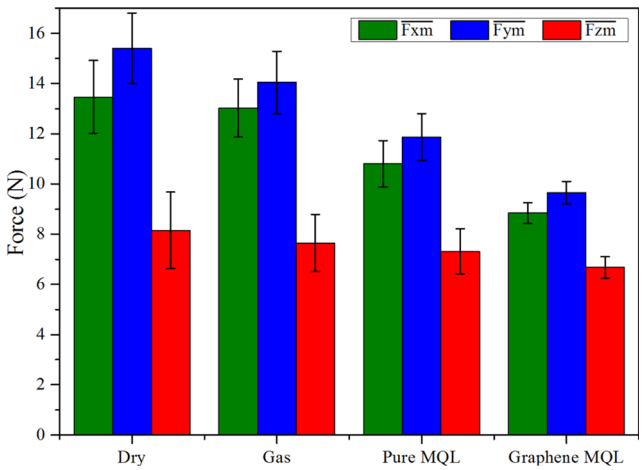

Fig. 12 The average of the positive and negative peak of measured milling force

separate the tool flank from the machined surface to reduce adhesion and built-up edge (see Fig. 19). In addition, the tool wear under the gas condition is smaller than that under the dry condition. This is because the gas takes away part of the milling heat and chip so that the tool wear is reduced. The tool wear under the graphene MQL condition is smaller than that under the pure MQL condition. This is because the graphene additive could enhance the lubrication and cooling performances of the oil film formed in the milling zone.

3.4 Surface integrity

The surface integrity of the workpiece is mainly influenced by factors such as milling force, milling temperature, and tool wear. The surface integrity directly determines the use performance and reliability of the workpiece. Therefore, the

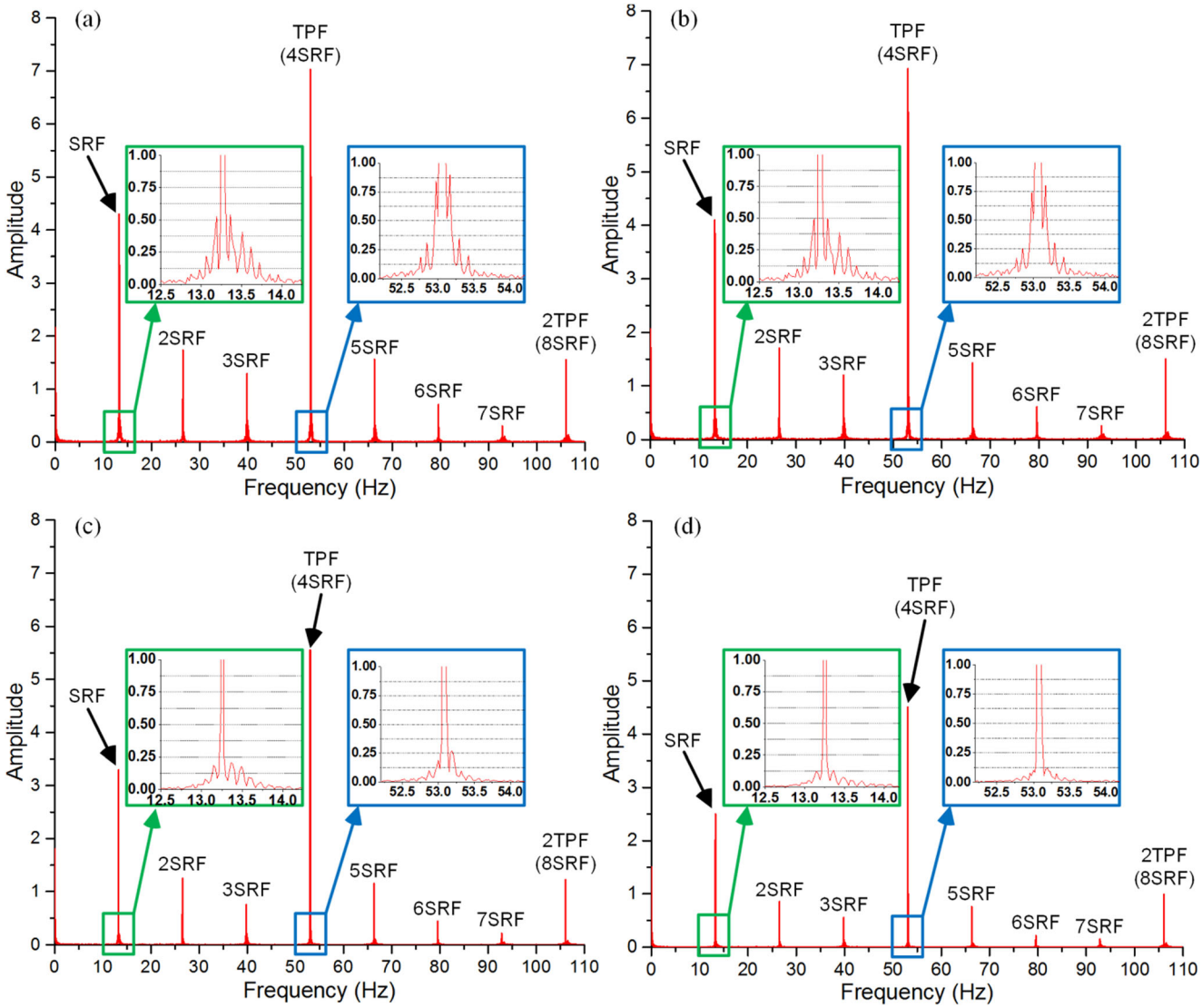

Fig. 13 The frequency spectra of the measured milling force signals ((**a**) dry, (**b**) gas, (**c**) pure MQL and (**d**) graphene MQL)

machined surface integrity is the most important evaluation parameter in the milling process.

The measured photos of the machined surface by the confocal microscope under the four cooling/lubrication conditions are shown in Fig. 20. In the dry and gas condition, adhesion, surface pit, large furrow, and feed mark were obviously observed. However, only feed mark was observed under the pure MQL and graphene MQL condition. In order to quantify the effects of the cooling/lubrication condition on the surface integrity, the surface roughness of the machined surface was measured, as shown in Fig. 21. The surface roughness of the machined surface in the dry condition is 0.653 μm, which is the largest in the four cooling/lubrication conditions. In the gas, pure MQL and graphene MQL condition, the surface roughness of the machined surface is 0.647, 0.425, and 0.311 μm, which is 0.92%, 34.92% and 52.37% smaller than that of the dry condition, respectively.

Among the four cooling/lubrication conditions, the surface quality achieved under the pure MQL and graphene MQL condition is much better than those obtained in the dry and gas condition. This is mainly because the oil films formed in the milling zone under the pure MQL and graphene MQL condition reduce the milling force, milling temperature, and tool wear. The larger milling force and milling temperature could cause surface pit and adhesion, the larger tool wear could cause large furrow and deteriorate surface quality. Meanwhile, the oil films formed in the milling zone could also separate the machined surface from the tool flank to reduce adhesion, surface pit, large furrow, and surface roughness (see Fig. 19). In addition, the surface quality achieved under the graphene MQL condition is much better than that obtained in the pure MQL condition. This could be explained by the fact that the graphene additive could enhance the lubrication and cooling performances of the oil film formed in milling zone.

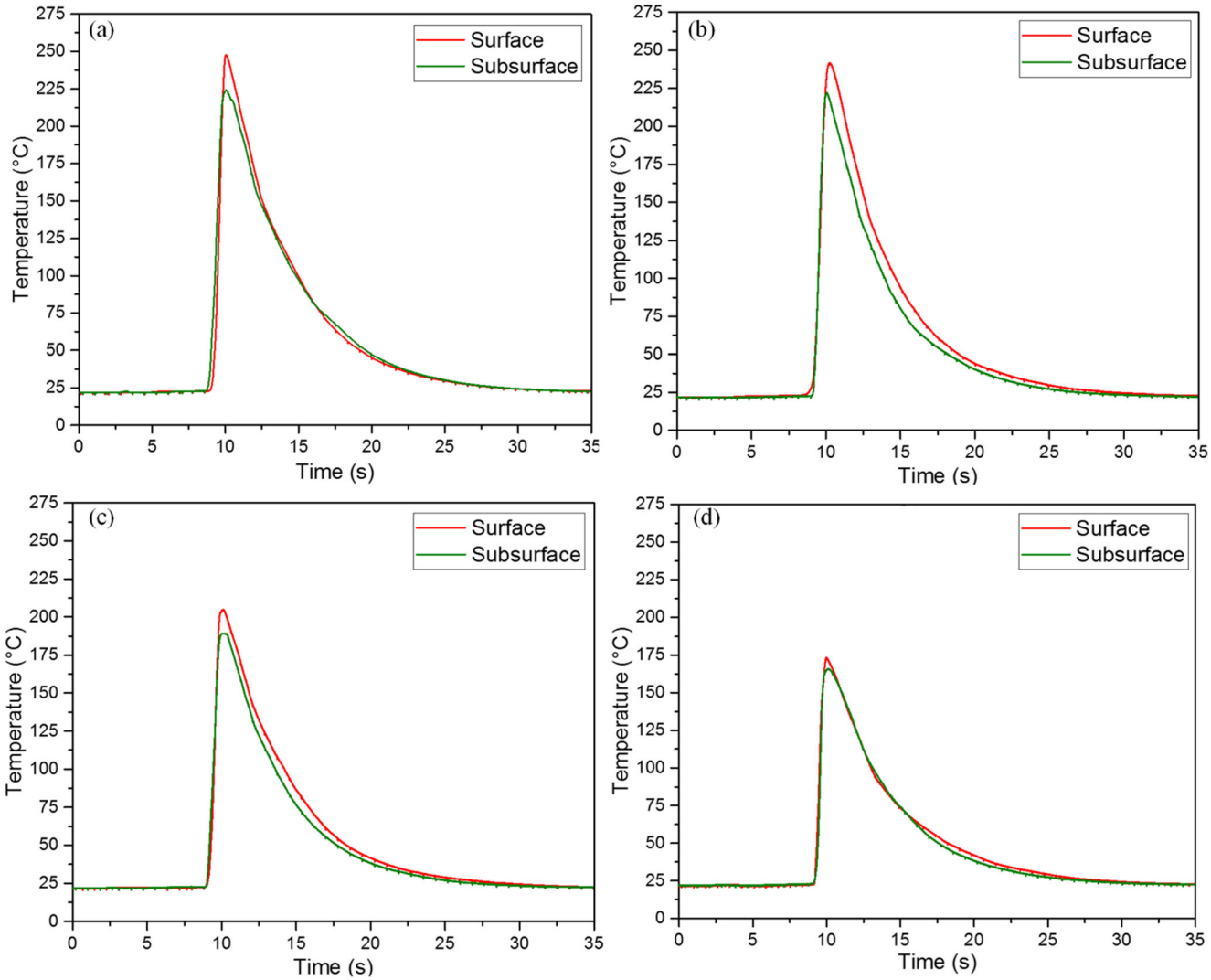

Fig. 14 The measured typical signal profiles of the surface temperature and the subsurface temperature ((**a**) dry, (**b**) gas, (**c**) pure MQL, and (**d**) graphene MQL)

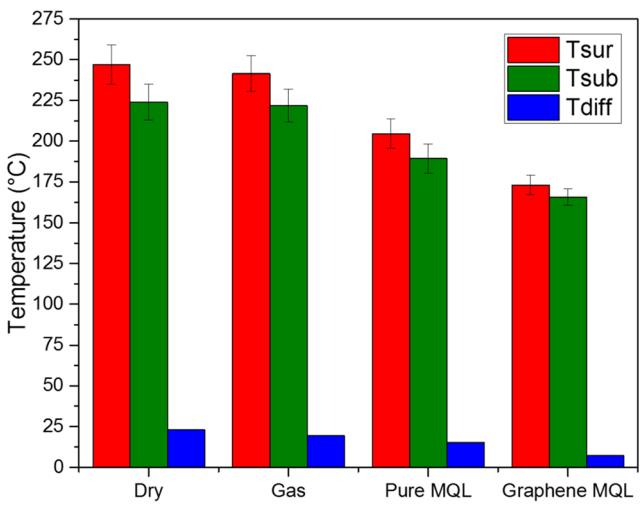

Fig. 15 The temperature peaks and the temperature differences

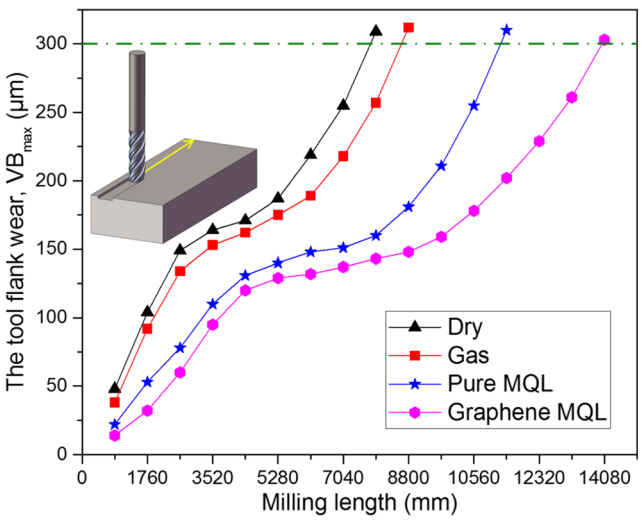

Fig. 16 The tool life curves under the four cooling/lubrication conditions

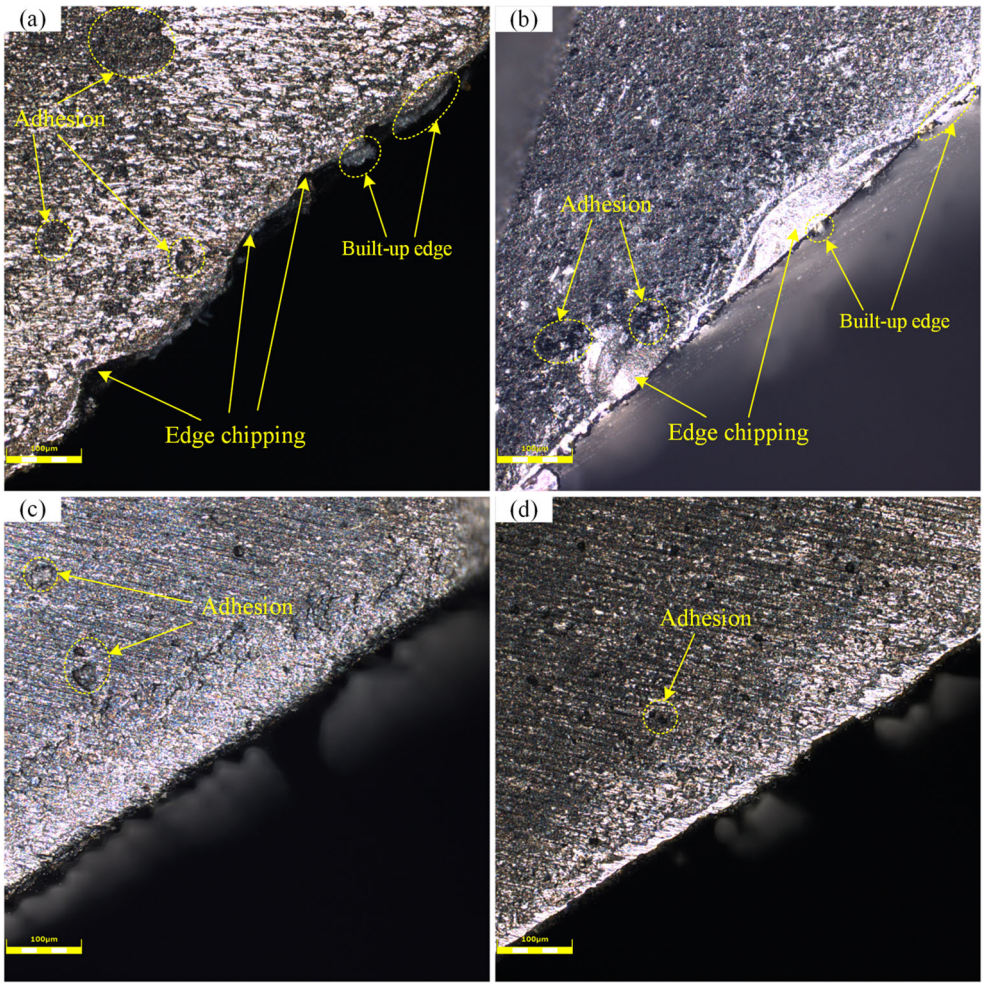

Fig. 17 The confocal microscope photos of the tool flank wear ((**a**) dry, (**b**) gas, (**c**) pure MQL, and (**d**) graphene MQL)

In addition, to further evaluate the effect of the cooling/lubrication condition on the surface integrity, the surface micro-hardness and the subsurface micro-hardness with the depth increasing to 200 μm under the four cooling/lubrication conditions were measured, as shown in Fig. 22. The micro-hardness variation trends with the depth increasing under each cooling/lubrication condition follow a similar rule: the surface micro-hardness is the largest, and with the depth increasing, the subsurface micro-hardness first decreases and then increases, and finally approaches the micro-hardness of the matrix material (312 HV). In the dry condition, the surface micro-hardness is 412.26 HV, which is the largest under the four cooling/lubrication conditions. In the gas, pure MQL, and graphene MQL condition, the surface micro-hardness is 406.93, 382.76, and 348.94 HV, which is 1.29%, 7.16%, and 15.36% smaller than that of the dry condition, respectively. In order to further evaluate the effect of the cooling/lubrication, condition on the subsurface hardening layer, the depth of the subsurface hardening layer was measured under each cooling/lubrication condition, as shown in Fig. 23. As shown in Fig. 24, the depth of the subsurface hardening layer in the dry condition is 148 μm, which is the largest under the four cooling/lubrication conditions. Under the gas, pure MQL, and graphene MQL condition, the depth of the subsurface hardening layer is 145, 116, and 81 μm, which is 2.03%, 21.62%, and 45.27% smaller than that of the dry condition, respectively.

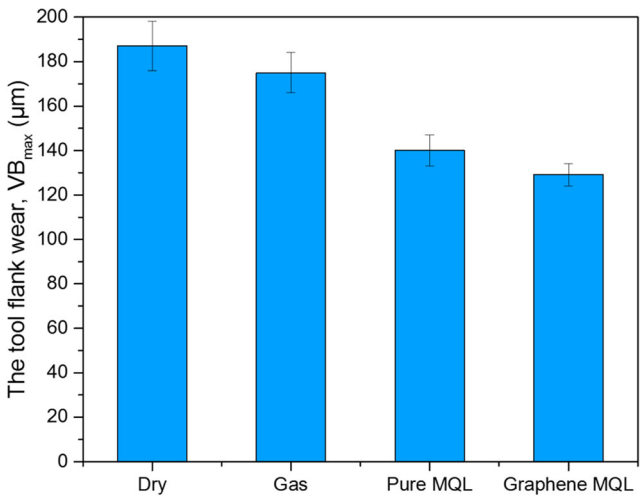

Fig. 18 The maximum width of the tool flank wear-land (VB_{max}) under the four cooling/lubrication conditions

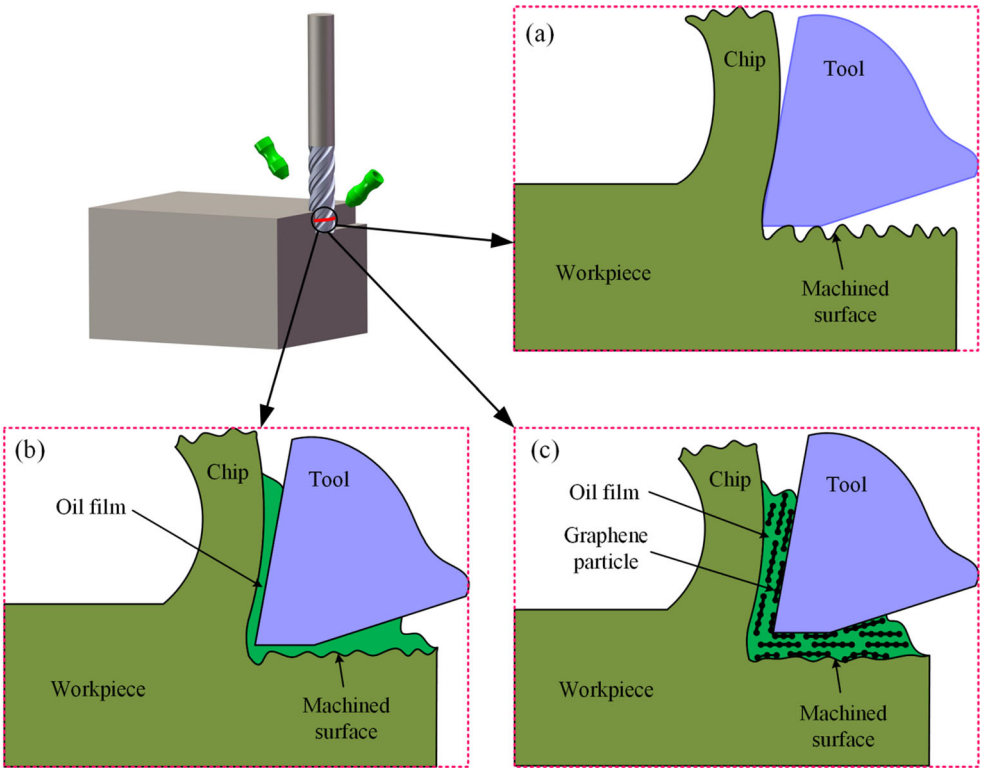

Fig. 19 Milling schematic under the four cooling/lubrication conditions ((**a**) dry and gas, (**b**) pure MQL, and (**c**) graphene MQL)

The work hardening in the milling process is mainly caused by the friction, the extrusion, and the milling heat generated in the tool-workpiece interface. Among them, the friction and the extrusion can strengthen the work hardening, while the milling heat could weaken the work hardening. For the four cooling/lubrication conditions, the surface micro-hardness is all larger than the micro-hardness of the matrix material. This may be due to the fact that the strengthening effect caused by the friction and the extrusion is stronger than the weakened effect caused by the milling heat on the machined surface. With the depth increasing the subsurface, micro-hardness first decreases and then increases, and finally approaches the micro-hardness of the matrix material. This is due to the superposition of the strengthening effect caused by the friction and the extrusion and the weakened effect caused by the milling heat at the different depth of the hardening layer. In addition, the depth of the subsurface hardening layer is significantly reduced under the pure MQL and graphene MQL condition. This is mainly because the oil film formed in the milling zone under the pure MQL and graphene MQL condition reduces the average friction coefficient, the milling force, and the milling temperature, as described in Section 3.1 and Section 3.2. The depth of the subsurface hardening layer under the graphene MQL condition is smaller than that of the pure MQL condition. This is mainly because the graphene additive could enhance the lubrication and cooling performances of the oil film formed in the milling zone so as to reduce the average friction coefficient, the milling force, and the milling temperature.

Overall, in this study, the machining characteristics in terms of milling force, milling temperature, tool wear, and surface integrity were improved in MQL milling with graphene-dispersed vegetable oil-based cutting fluid. Meanwhile, in the existing researches, the nanoparticle-dispersed vegetable oil-based cutting fluids have been used in turning and grinding process. In turning process, the cutting force and temperature were decreased significantly by using the MQL with graphite-dispersed vegetable oil-based cutting fluid [19]. In grinding process, the machining performances in terms of grinding forces, grinding temperatures, and surface integrity were improved significantly by using the MQL with CuO-dispersed vegetable oil-based cutting fluid [20]. Therefore, the nanoparticle-dispersed vegetable oil-based cutting fluids are effective for improving the machining performances. In addition, the application of the graphene-dispersed vegetable oil-based cutting fluid in turning and grinding process is also very promising.

4 Conclusion

In this study, the milling characteristics of TC4 under the four cooling/lubrication conditions (dry, gas, pure MQL, graphene MQL) are experimentally investigated. In particular, the effects of the graphene additive on milling force, milling temperature, tool wear, and surface integrity are analyzed. The research results could give a feasibility and

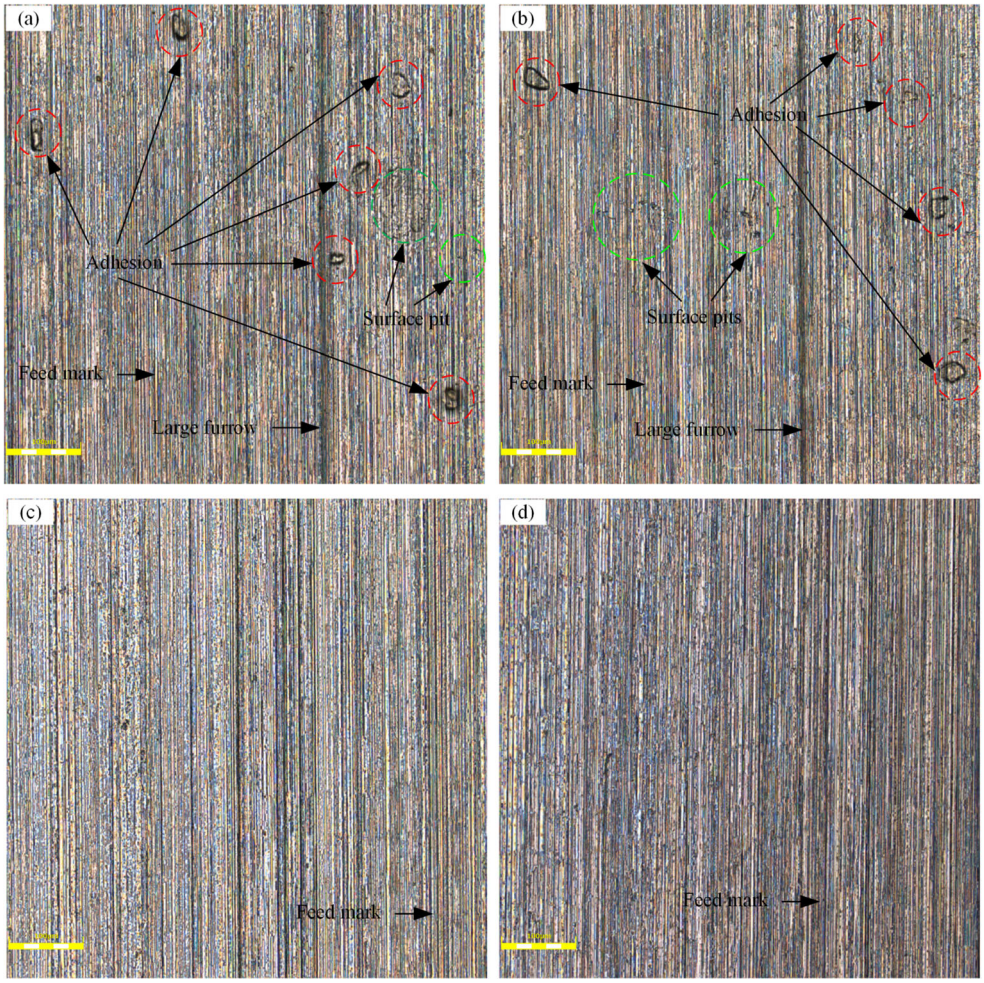

Fig. 20 The confocal microscope photos of the machined surface ((**a**) dry, (**b**) gas, (**c**) pure MQL, and (**d**) graphene MQL)

some experimental basis for the application of the graphene additive in MQL milling. The following conclusions could be drawn.

(1) The graphene-dispersed cutting fluid is prepared by a two-step method using a magnetic stirrer and an ultrasonic dispersion instrument. After standing for 12 h, an

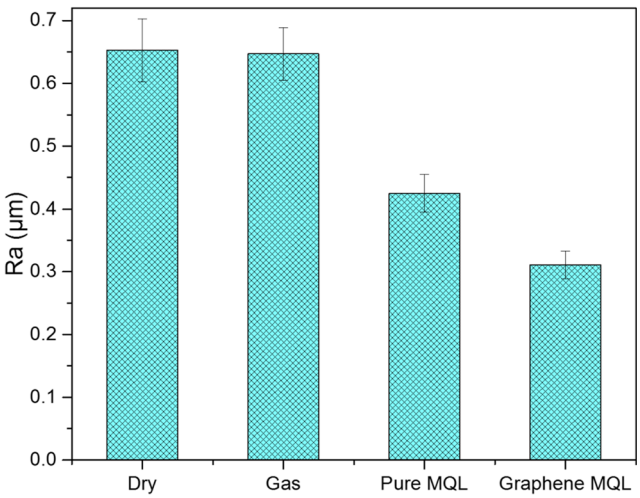

Fig. 21 The surface roughness of the machined surface

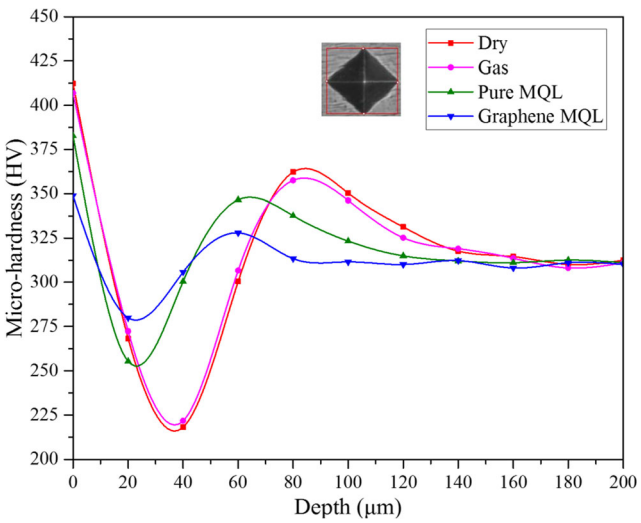

Fig. 22 The surface micro-hardness and the subsurface micro-hardness

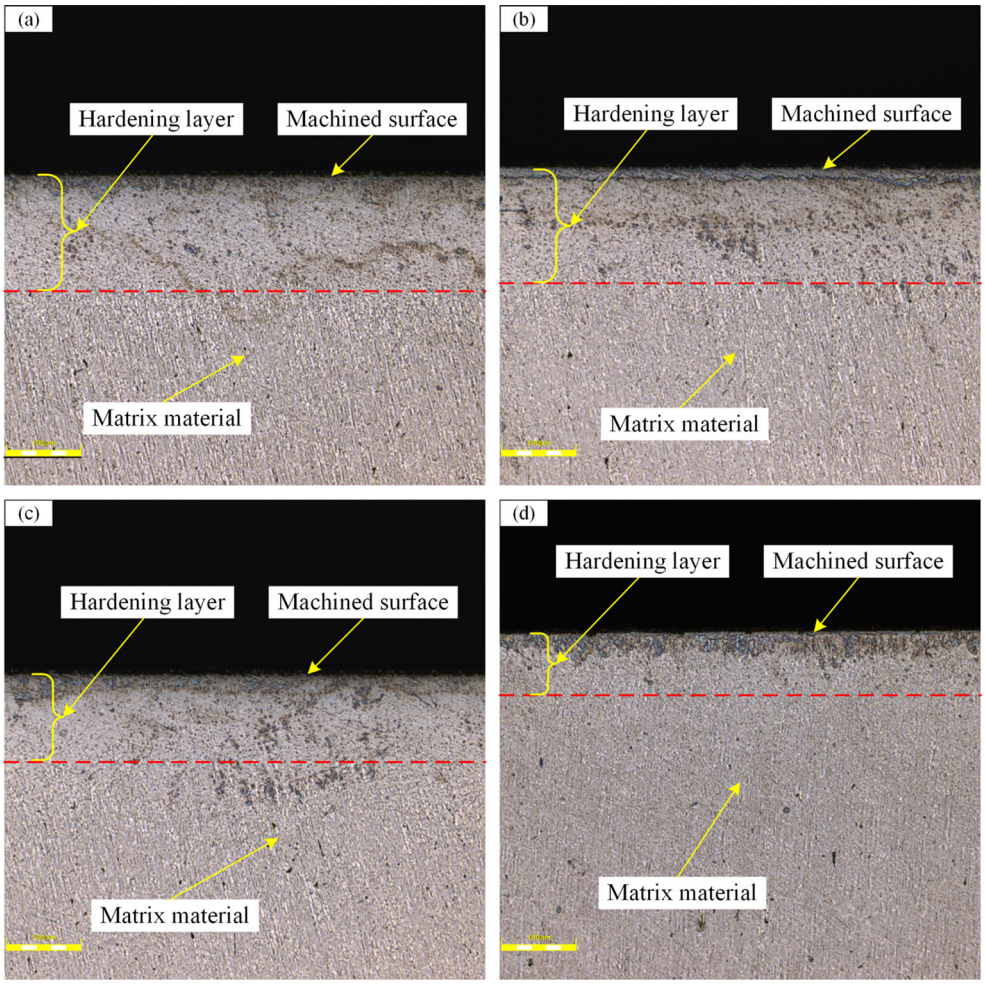

Fig. 23 The depth of the subsurface hardening layer ((**a**) dry, (**b**) gas, (**c**) pure MQL, and (**d**) graphene MQL)

obvious sedimentation phenomenon is not observed in the graphene-dispersed cutting fluid. Especially in the whole experiment, the sedimentation phenomenon is also not found. Therefore, the preparation method of graphene-dispersed cutting fluid is feasible and effective.

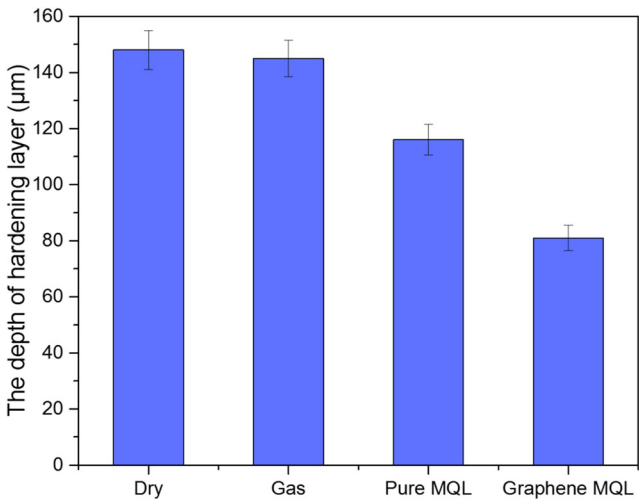

Fig. 24 The depth of the subsurface hardening layer

(2) While applying the graphene MQL to the milling process, the milling force is significantly decreased. This is likely because the graphene additive could enhance the anti-friction and load-bearing capacity of the oil film formed in the milling zone. In addition, the vibration intensity of the milling process is also significantly reduced under the graphene MQL condition. This could be explained that the graphene additive could also enhance the damping effect of the oil film formed in the milling zone.

(3) Regarding the milling temperature, both the surface temperature peak and the subsurface temperature peak are significantly reduced under the graphene MQL condition. Meanwhile, the difference between the surface temperature peak and the subsurface temperature peak is also significantly decreased. This is likely because the graphene additive could enhance the cooling capacity of the oil film formed in milling zone based on the theory of solid enhancing heat transfer.

(4) Regarding the tool wear, the tool life in the graphene MQL condition is the largest among the four cooling/lubrication conditions. Meanwhile, adhesion, edge

chipping, and built-up edge are significantly reduced under the graphene MQL condition. In addition, the graphene MQL condition shows the smallest tool flank wear-land among the four cooling/lubrication conditions. Overall, this is because the graphene additive could enhance the lubrication and cooling performances of the oil film formed in the milling zone.

(5) Regarding the surface integrity, it is significantly improved when applying the graphene MQL to the milling process. Adhesion, surface pit, and large furrow are significantly reduced because the oil films formed in the milling zone could separate the machined surface from the tool flank. Meanwhile, the surface roughness of the graphene MQL condition is the smallest among the four cooling/lubrication conditions. In addition, the surface micro-hardness and the depth of the subsurface hardening layer are significantly reduced under the graphene MQL condition. On the whole, this could be explained by the fact that the graphene additive could enhance the lubrication and cooling performances of the oil film formed in the milling zone so as to reduce the average friction coefficient, the milling force, and the milling temperature.

(6) Overall, the graphene additive is effective for improving the machining performances by improving the cooling and lubrication characteristics of the vegetable oil-based cutting fluid. Therefore, the application of the graphene-dispersed vegetable oil-based cutting fluid in machining process is very promising.

Acknowledgements The authors would like to thank Professor Lida Zhu for excellent technical support and Hongxiao Li for critically reviewing the manuscript.

Funding information This work was supported by grants from the Major Project of Ministry of Industry and Information Technology of China (201675514), the Joint Funds of the National Natural Science Foundation of China (U1508206), and the Key Laboratory Special Project of Shenyang City (F15153100).

References

1. Mark Benjamin D, Sabarish VN, Hariharan MV, Samuel Raj D (2018) On the benefits of sub-zero air supplemented minimum quantity lubrication systems: an experimental and mechanistic investigation on end milling of Ti-6-Al-4-V alloy. Tribol Int 119:464–473. https://doi.org/10.1016/j.triboint.2017.11.021
2. Lawal SA, Choudhury IA, Nukman Y (2012) Application of vegetable oil-based metalworking fluids in machining ferrous metals—a review. Int J Mach Tools Manuf 52(1):1–12. https://doi.org/10.1016/j.ijmachtools.2011.09.003
3. Wang Y, Li C, Zhang Y, Yang M, Li B, Jia D, Hou Y, Mao C (2016) Experimental evaluation of the lubrication properties of the wheel/workpiece interface in minimum quantity lubrication (MQL) grinding using different types of vegetable oils. J Clean Prod 127:487–499. https://doi.org/10.1016/j.jclepro.2016.03.121
4. Pervaiz S, Rashid A, Deiab I, Nicolescu CM (2016) An experimental investigation on effect of minimum quantity cooling lubrication (MQCL) in machining titanium alloy (Ti6Al4V). Int J Adv Manuf Technol 87(5):1371–1386. https://doi.org/10.1007/s00170-016-8969-6
5. Gajrani KK, Ram D, Sankar MR (2017) Biodegradation and hard machining performance comparison of eco-friendly cutting fluid and mineral oil using flood cooling and minimum quantity cutting fluid techniques. J Clean Prod 165:1420–1435. https://doi.org/10.1016/j.jclepro.2017.07.217
6. Khan MMA, Mithu MAH, Dhar NR (2009) Effects of minimum quantity lubrication on turning AISI 9310 alloy steel using vegetable oil-based cutting fluid. J Mater Process Technol 209(15):5573–5583. https://doi.org/10.1016/j.jmatprotec.2009.05.014
7. Priarone PC, Robiglio M, Settineri L, Tebaldo V (2014) Milling and turning of titanium aluminides by using minimum quantity lubrication. Procedia CIRP 24:62–67. https://doi.org/10.1016/j.procir.2014.07.147
8. Rahim EA, Sasahara H (2011) A study of the effect of palm oil as MQL lubricant on high speed drilling of titanium alloys. Tribol Int 44(3):309–317. https://doi.org/10.1016/j.triboint.2010.10.032
9. Choi SUS, Eastman JA (1995) Enhancing thermal conductivity of fluids with nanoparticles. Asme Fed 231(1):99–105
10. Wang Y, Li C, Zhang Y, Li B, Yang M, Zhang X, Guo S, Liu G, Zhai M (2017) Comparative evaluation of the lubricating properties of vegetable-oil-based nanofluids between frictional test and grinding experiment. J Manuf Process 26:94–104. https://doi.org/10.1016/j.jmapro.2017.02.001
11. Sharma AK, Tiwari AK, Dixit AR (2016) Effects of minimum quantity lubrication (MQL) in machining processes using conventional and nanofluid based cutting fluids: a comprehensive review. J Clean Prod 127:1–18. https://doi.org/10.1016/j.jclepro.2016.03.146
12. Padgurskas J, Rukuiza R, Prosyčevas I, Kreivaitis R (2013) Tribological properties of lubricant additives of Fe, Cu and Co nanoparticles. Tribol Int 60:224–232. https://doi.org/10.1016/j.triboint.2012.10.024
13. Shabgard M, Seyedzavvar M, Mohammadpourfard M (2017) Experimental investigation into lubrication properties and mechanism of vegetable-based CuO nanofluid in MQL grinding. Int J Adv Manuf Technol 92(9):3807–3823. https://doi.org/10.1007/s00170-017-0319-9
14. Lee P-H, Nam JS, Li C, Lee SW (2012) An experimental study on micro-grinding process with nanofluid minimum quantity lubrication (MQL). Int J Precis Eng Manuf 13(3):331–338. https://doi.org/10.1007/s12541-012-0042-2
15. Kalita P, Malshe AP, Arun Kumar S, Yoganath VG, Gurumurthy T (2012) Study of specific energy and friction coefficient in minimum quantity lubrication grinding using oil-based nanolubricants. J Manuf Process 14(2):160–166. https://doi.org/10.1016/j.jmapro.2012.01.001
16. Li B, Li C, Zhang Y, Wang Y, Yang M, Jia D, Zhang N, Wu Q (2017) Effect of the physical properties of different vegetable oil-based nanofluids on MQLC grinding temperature of Ni-based alloy. Int J Adv Manuf Technol 89(9):3459–3474. https://doi.org/10.1007/s00170-016-9324-7
17. Kim JS, Kim JW, Lee SW (2017) Experimental characterization on micro-end milling of titanium alloy using nanofluid minimum quantity lubrication with chilly gas. Int J Adv Manuf Technol 91(5):2741–2749. https://doi.org/10.1007/s00170-016-9965-6
18. Park KH, Ewald B, Kwon PY (2011) Effect of nano-enhanced lubricant in minimum quantity lubrication balling milling. J Tribol 133(3):3526–3537

19. Su Y, Gong L, Li B, Liu Z, Chen D (2016) Performance evaluation of nanofluid MQL with vegetable-based oil and ester oil as base fluids in turning. Int J Adv Manuf Technol 83(9):2083–2089. https://doi.org/10.1007/s00170-015-7730-x
20. Jia D, Li C, Zhang D, Zhang Y, Zhang X (2014) Experimental verification of nanoparticle jet minimum quantity lubrication effectiveness in grinding. J Nanopart Res 16(12):2758. https://doi.org/10.1007/s11051-014-2758-7
21. Sayuti M, Sarhan AAD, Tanaka T, Hamdi M, Saito Y (2013) Cutting force reduction and surface quality improvement in machining of aerospace duralumin AL-2017-T4 using carbon onion nanolubrication system. Int J Adv Manuf Technol 65(9):1493–1500. https://doi.org/10.1007/s00170-012-4273-2
22. Sarhan AAD, Sayuti M, Hamdi M (2012) Reduction of power and lubricant oil consumption in milling process using a new SiO 2 nanolubrication system. Int J Adv Manuf Technol 63(5–8):505–512
23. Sayuti M, Erh OM, Sarhan AAD, Hamdi M (2014) Investigation on the morphology of the machined surface in end milling of aerospace AL6061-T6 for novel uses of SiO2 nanolubrication system. J Clean Prod 66:655–663. https://doi.org/10.1016/j.jclepro.2013.11.058
24. Balandin AA, Ghosh S, Bao W, Calizo I, Teweldebrhan D, Miao F, Lau CN (2008) Superior thermal conductivity of single-layer graphene. Nano Lett 8(3):902–907
25. Berman D, Erdemir A, Sumant AV (2014) Graphene: a new emerging lubricant. Mater Today 17(1):31–42
26. Hu Z-Y, Cheng X-W, Li S-L, Zhang H-M, Wang H, Zhang Z-H, Wang F-C (2017) Investigation on the microstructure, room and high temperature mechanical behaviors and strengthening mechanisms of the (TiB+TiC)/TC4 composites. J Alloys Compd 726:240–253. https://doi.org/10.1016/j.jallcom.2017.08.017
27. Che Sidik NA, Mahmud Jamil M, Aziz Japar WMA, Muhammad Adamu I (2017) A review on preparation methods, stability and applications of hybrid nanofluids. Renew Sust Energ Rev 80:1112–1122. https://doi.org/10.1016/j.rser.2017.05.221
28. Fuskele V, Sarviya RM (2017) Recent developments in nanoparticles synthesis, preparation and stability of nanofluids. Mater. Today: Proceedings 4(2, Part A):4049–4060. https://doi.org/10.1016/j.matpr.2017.02.307
29. Ghani JA, Che Haron CH, Hamdan SH, Md Said AY, Tomadi SH (2013) Failure mode analysis of carbide cutting tools used for machining titanium alloy. Ceram Int 39(4):4449–4456. https://doi.org/10.1016/j.ceramint.2012.11.038
30. Altintas Y (2012) Manufacturing Automation: Metal Cutting Mechanics, Machine Tool Vibrations, and CNC design, 2nd edn. Cambridge University Press Cambridge.
31. Liu Z, Chen M, An Q (2015) Investigation of friction in end-milling of Ti-6Al-4V under different green cutting conditions. Int J Adv Manuf Technol 78(5):1181–1192. https://doi.org/10.1007/s00170-014-6730-6
32. Huang PL, Li JF, Sun J, Jia XM (2016) Cutting signals analysis in milling titanium alloy thin-part components and non-thin-wall components. Int J Adv Manuf Technol 84(9):2461–2469. https://doi.org/10.1007/s00170-015-7837-0
33. Zhong W, Zhao D, Wang X (2010) A comparative study on dry milling and little quantity lubricant milling based on vibration signals. Int J Mach Tools Manuf 50(12):1057–1064. https://doi.org/10.1016/j.ijmachtools.2010.08.011